The Astrophysical Journal Letters, 851:L10 (6pp), 2017 December 10 https://doi.org/10.3847/2041-8213/aa9c3e
© 2017. The American Astronomical Society. All rights reserved.

The First Detection of a Pulsar with ALMA

R. P. Mignani[1,2], R. Paladino[3], B. Rudak[4], A. Zajczyk[5], A. Corongiu[6], A. de Luca[1], W. Hummel[7], A. Possenti[6], U. Geppert[2], M. Burgay[6], and G. Marconi[8]
[1] INAF—Istituto di Astrofisica Spaziale e Fisica Cosmica Milano, via E. Bassini 15, I-20133 Milano, Italy
[2] Janusz Gil Institute of Astronomy, University of Zielona Góra, Lubuska 2, 65-265, Zielona Góra, Poland
[3] INAF—Istituto di Radioastronomia and Italian ALMA Regional Centre, via P. Gobetti 101, I-40129 Bologna, Italy
[4] Nicolaus Copernicus Astronomical Center, Polish Academy of Sciences, ul. Rabiańska 8, 87100, Toruń, Poland
[5] University of Iowa, Department of Physics and Astronomy, 203, Van Allen Hall, Iowa City, IA 52242, USA
[6] INAF Osservatorio Astronomico di Cagliari, Via della Scienza 5, I-09047 Selargius, Italy
[7] European Southern Observatory, Karl Schwarzschild-Str. 2, D-85748 Garching, Germany
[8] European Southern Observatory, Alonso de Cordova 3107 Vitacura, Santiago de Chile, Chile
Received 2017 October 11; revised 2017 November 17; accepted 2017 November 20; published 2017 December 6

Abstract

Although there is a general consensus on the fact that pulsars' radio emission is coherent in nature, whereas the emission from the optical to high-energy γ-rays is due to incoherent processes, it has not been established yet at which wavelengths the transition occurs, which is key information for all emission models of pulsar magnetospheres. Of course, to address this issue, covering the spectral region between the GHz radio frequencies and the mid-infrared (IR) is crucial. We used the Atacama Large Millimeter/submillimeter Array (ALMA) to observe the Vela pulsar (PSR B0833−45), one of the very few observed in radio and from the mid-IR up to the very high-energy γ-rays. We detected Vela at frequencies of 97.5, 145, 233, and 343.5 GHz, which makes it the first pulsar ever detected with ALMA. Its energy density spectrum follows a power law of spectral index $\alpha = -0.93 \pm 0.16$. This corresponds to very high brightness temperatures—from 10^{17} to 10^{15} K—suggesting that a coherent radiative process still contributes to the millimeter/submillimeter emission. Therefore, this is the first indication of coherent emission in pulsars extending to the submillmeter range. At the same time, we identified an extended structure, preliminarily detected in ground-based near-IR observations, at a distance of $\sim 1\farcs4$ from the pulsar, possibly interpreted as a counter-jet protruding from the pulsar.

Key words: pulsars: individual (Vela pulsar)

1. Introduction

The Vela pulsar (PSR B0833−45), in the Vela supernova remnant, is a relatively young isolated neutron star, with a characteristic age $\tau \approx 11{,}000$ years, estimated from the ratio between its spin-down period P_s (89 ms) and its derivative $\dot{P}_s$ (12.5×10^{-14} s s^{-1}) as $\tau = P_s/(2\dot{P}_s)$. According to the magnetic dipole model (e.g., Pacini 1968), the timing parameters (Manchester et al. 2005) yield a surface magnetic field $B_s = 3.38 \times 10^{12}$ G and a rotational energy loss rate $\dot{E} = 6.96 \times 10^{36}$ erg s^{-1}. The Vela pulsar was discovered in the radio band in 1968 (Large et al. 1968) and soon after it was detected both in the X- (Harnden & Gorenstein 1973) and γ-rays (Thompson et al. 1975) and, later on, also in the optical band (Lasker 1976; Wallace et al. 1977). Vela was also detected in the near-ultraviolet (UV) with the *HST* (Romani et al. 2005), the near-infrared (IR) with the VLT (Shibanov et al. 2003), and the mid-IR with *Spitzer* (Danilenko et al. 2011) becoming, aside from PSR B0531+21 in the Crab Nebula, the only radio pulsar detected all the way from the mid-IR up to γ-ray energies above 50 GeV, thanks to *Fermi* observations (Leung et al. 2014).

The Vela pulsar spectral energy distribution (SED) is quite complex. In the soft X-ray band (0.1–2 keV), the SED features a thermal component ascribed to emission from the cooling neutron star surface (Manzali et al. 2007). The rest of the SED is purely nonthermal and is characterized by the combination of different power-law (PL) spectra $F_\nu \propto \nu^\alpha$, where F_ν is the flux density per unit frequency ν, with turnovers between different energy bands. In particular, a spectral turnover is observed in the radio band at frequencies above a few gigahertz, perhaps associated with the transition between coherent and incoherent emission processes, with the former responsible for the radio emission and the latter for the nonthermal emission from the near-IR up to the high-energy γ-rays.

Determining the frequency range where such a transition occurs provides key information for the radiation emission models in pulsar magnetospheres. Of course, the knowledge of the pulsar spectrum in the spectral region between millimeter and micron wavelengths, i.e., between the high-frequency radio band and the mid-IR, is crucial to constrain the value of the transition frequency. Being one of the three pulsars detected in the mid-IR, with the Crab (Temim et al. 2009) and, possibly, Geminga (Danilenko et al. 2011), Vela is an obvious target for observations with the Atacama Large Millimeter/submillimeter Array (ALMA), the most sensitive telescope in the 3.6–0.3 mm range.

This manuscript is divided as follows. Observations and data analysis are described in Section 2, whereas the results are presented and discussed in Sections 3 and 4, respectively. A summary and conclusions then follow in Section 5.

2. Observations and Data Reduction

We observed the Vela pulsar with ALMA during Cycle 3, from 2016 March to July, in four different frequency bands: Band 3 (97.5 GHz), Band 4 (145 GHz), Band 6 (233 GHz), and Band 7 (343.5 GHz), corresponding to wavelengths of 3.07, 2.07, 1.28, and 0.87 mm, respectively. Our ALMA observations were executed with the 12 m array, with an average of 38 antennas, in different configurations, with maximum baselines

Table 1
Summary of the ALMA Observations of the Vela Pulsar

Band	ν (GHz)	Date (2016)	Time (minutes)	Beam (arcsec × arcsec)	rms (μJy/beam)	Flux Density (μJy)
3	97.5	Jul 23	22	0.75 × 0.68	25	252 ± 35
4	145	Jul 14	22	0.77 × 0.74	20	170 ± 26
6	233	Apr 17	46	0.88 × 0.73	18	122 ± 22
7	343.5	Mar 10, 26, 28	120	0.66 × 0.49	18	67 ± 19

Note. Columns report the observing band, its central frequency ν, the observation date, the integration time, the size of the synthesized beam, rms, and the measured pulsar flux density. We included the error on the absolute ALMA flux calibration, estimated to be ∼10%, as discussed in Section 2 (see also Fomalont et al. 2014).

ranging from 495 m (Band 7) to 867 m (Band 3), allowing a spatial resolution ranging from ∼0.″6 to 0.″8. The total time spent on the target was ∼3.3 hr, which provided a 1σ sensitivity of ∼20 μJy/beam in each of the selected bands. Table 1 reports the details of each observation. The 12 m array correlator was configured to allow observations in dual polarization in a 7.5 GHz wide band, divided into four spectral windows (1.875 GHz each), with 128 channels, ∼15 MHz wide. For each band, standard frequencies ν have been used, which are optimized to achieve the best atmospheric transmission. The observed field of view decreases with the frequency and ranges from 63.″4 in Band 3–18″ in Band 7. Raw data were calibrated using the Common Astronomy Software Applications (CASA) software package (version 4.5.3) and the ALMA pipeline (Pipeline-Cycle3-R4-B). To set the flux density scale for the Band 4, 6, and 7 observations, we used flux measurements of the quasar J1107−4449. The flux density uncertainty on this calibrator reported in the ALMA Calibrator Source Catalog[9] is 10%. For the Band 3 observations, we fixed the flux density scale using data from Callisto observations, and using the Butler-JPL-Horizons 2012 standard model. We conservatively assume the uncertainty on the flux density to be 10%. For the astrometry calibration, we used as a reference the radio position of the quasar J0811−4929 at $\alpha = 08^{h}11^{m}08\overset{s}{.}803$ (±0.″0058); $\delta = -49°29'43\overset{''}{.}509$ (±0.″0021) at about 6° from our target, as reported in the ALMA Calibrator Source Catalog. We produced images from the calibrated data using the task `clean` in CASA. The images were generated using "natural" weighting, in order to maximize the sensitivity. For all images, we computed the pulsar position at the epochs of our ALMA observations using its radio coordinates as a reference (Dodson et al. 2003), $\alpha = 08^{h}35^{m}20\overset{s}{.}61$; $\delta = -45°10'34\overset{''}{.}87$ (epoch 2000.0), and correcting them for its radio proper motion (Dodson et al. 2003), $\mu_{\alpha} = -49.6$ mas yr^{-1} and $\mu_{\delta} = +29.9$ mas yr^{-1}. The uncertainties on the radio proper motion and pulsar position are negligible and they do not affect the precision on the pulsar position determination on the ALMA images. The astrometric accuracy in the different bands, taken into account the signal-to-noise (S/N) and the resolution, is 56, 48, 43, and 123 mas, in Bands 3, 4, 6, and 7, respectively.

3. Results

The ALMA images in Bands 3, 4, and 6 clearly show a source at a position coincident with the radio coordinates of the Vela pulsar, corrected for its proper motion (Dodson et al. 2003). Figure 1 shows the ALMA Band 7 image with the source intensity contours from the Band 3, 4, and 6 images

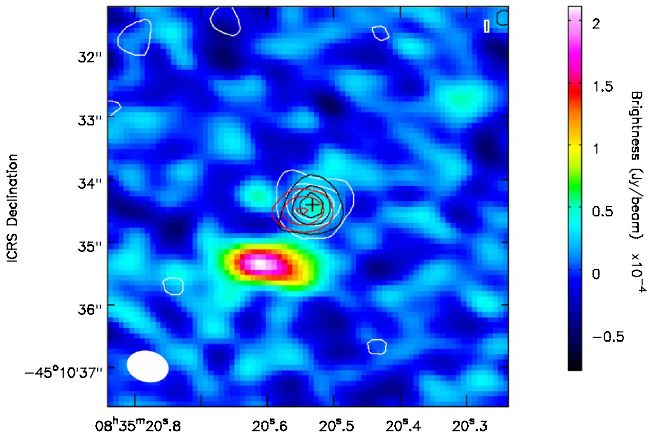

Figure 1. Image of the Vela pulsar field taken with ALMA in Band 7 (343.5 GHz). The intensity contours overlaid at the center of the image correspond to the pulsar detections in Band 3 (97.5 GHz; white), Band 4 (145 GHz; black), and Band 6 (233 GHz; red). The contours correspond to 3, 6, and 8σ levels for the Band 3 and 4 images, and to 3, 4, and 4.8σ levels for the Band 6 image. The filled ellipse in the left corner represents the size of the synthesized beam of the Band 7 image. The extended source about 1.″4 southeast of the pulsar is the nebula discussed in Section 4.2. The cross indicates the pulsar position at the average epoch of our ALMA observations.

overlaid, which shows that the source has been detected in all bands. In all images, its brightness profile is consistent with the instrument point-spread function (PSF), as expected from a point source. The accuracy of the ALMA absolute astrometry makes us confident that we can claim the pulsar identification based upon positional coincidence. The pulsar is clearly detected, with flux densities of 252 ± 35, 170 ± 26, and 122 ± 22 μJy in Bands 3, 4, and 6, respectively, including both statistical errors and the uncertainty on the ALMA absolute flux calibration. It has also been detected in Band 7, although with a lower significance (S/N ∼ 3.7) and a flux density of 67 ± 19 μJy. We measured the pulsar flux density in the four ALMA bands within a square aperture of 1″ size centered on its position by fitting an elliptical Gaussian to the source brightness profile.

The flux densities of the Vela pulsar in the four ALMA bands (Table 1) can be fitted by a PL with spectral index $\alpha = -0.93 \pm 0.16$ ($\chi^2 = 0.7$). This clearly indicates that the pulsar emission in the millimeter/submillimeter range is nonthermal in origin, like in the optical/UV (Romani et al. 2005) and in the near-IR (Shibanov et al. 2003; Danilenko et al. 2011), and is produced in the neutron star magnetosphere.

An additional, extended, and bright source is also visible 1.″4 southeast of the pulsar. This source (hereafter, the "nebula") is only detected in Band 7, where it is relatively bright with a flux

[9] https://almascience.eso.org/sc/

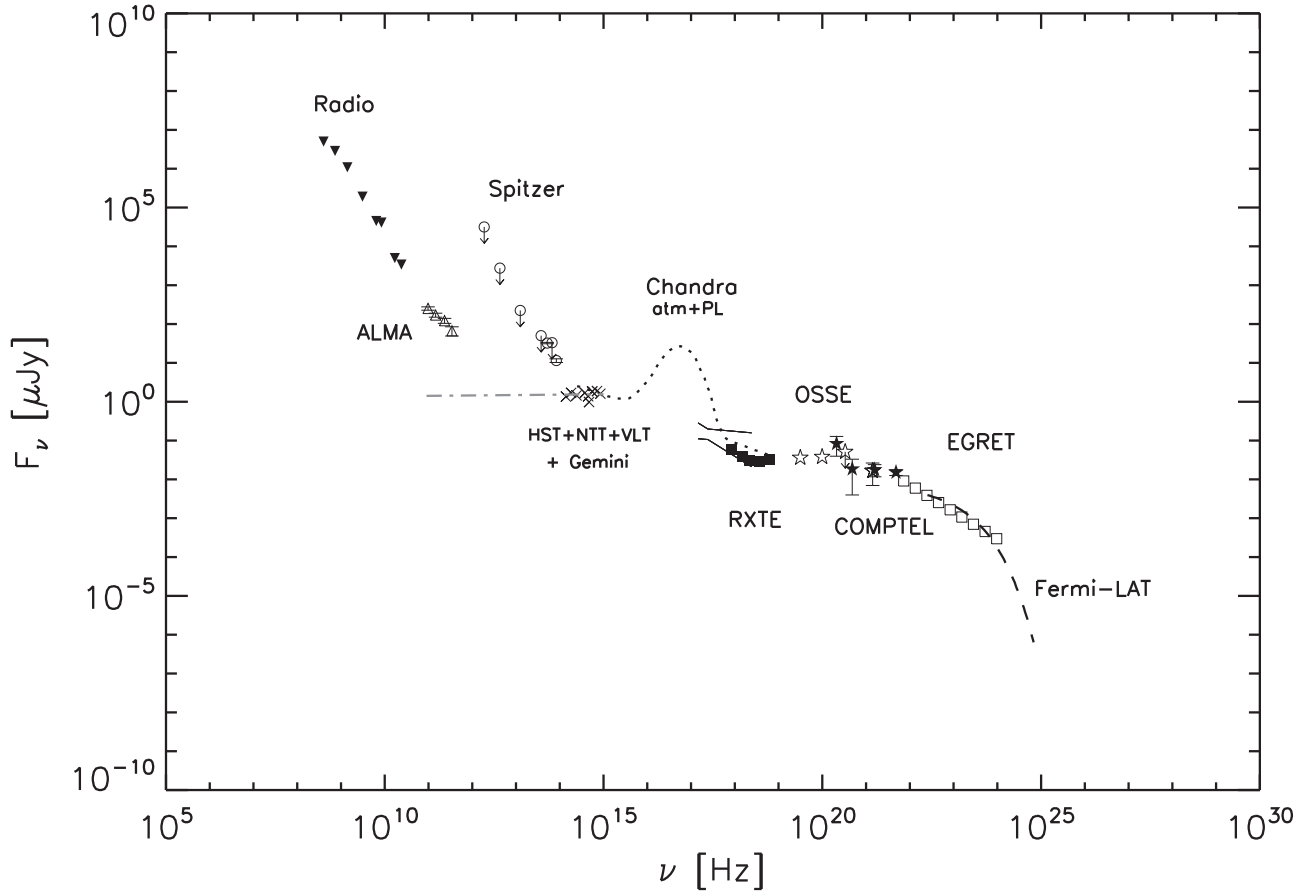

Figure 2. Vela pulsar SED from the radio to the γ-rays. The radio data (filled inverted triangles) come from Manchester et al. (2005), Johnston et al. (2006), Keith et al. (2011), and S. Johnston (2017, private communication). The open triangles with the error bars are our ALMA data (see Table 1). The rest of the spectrum is built from measurements collected from the literature (see Danilenko et al. 2011; Zyuzin et al. 2013, and references therein). The dotted–dashed line is the extrapolation of the near-UV–optical–near-IR PL spectrum (Zyuzin et al. 2013) toward the ALMA bands. The dashed line is the best-fit PL plus exponential cut-off γ-ray spectrum derived from the *Fermi* data (Acero et al. 2015).

of $278 \pm 33\,\mu$Jy computed down to a 5σ intensity contour, where the σ is $18\,\mu$Jy/beam (Table 1).

4. Discussion

4.1. The Pulsar

We compared the ALMA spectrum with the radio spectrum below 24 GHz (Figure 2). The latter is presented for eight flux density values in the frequency range between 400 MHz and 24 GHz (Manchester et al. 2005; Johnston et al. 2006; Keith et al. 2011). The spectrum has been recently classified as a broken PL, with the break frequency around 900 MHz, and the spectral index $\alpha = -2.24 \pm 0.09$ above the break (Jankowski et al. 2018). As shown above, the ALMA spectrum follows a PL with spectral index $\alpha = -0.93 \pm 0.16$, i.e., it is much flatter than the neighboring radio spectrum. The gap between the two spectra is quite wide, but likely it can be closed smoothly by, e.g., a future detection of Vela at 40 GHz (Band 1) with ALMA. In the radio domain, the maximal flux density ($\sim$5 Jy) is achieved at $\sim$400 MHz, which yields a brightness temperature $T_{\rm b} \gtrsim 10^{27}$ K for an emitting region smaller than one neutron star radius. Under this assumption, $T_{\rm b}$ would be $\gtrsim 10^{17}$ K and $\gtrsim 10^{15}$ K, in the ALMA Bands 3 and 7, respectively, implying coherence. Lower, but still quite high, values of $T_{\rm b}$ would be derived if the size of the emission region were, instead, a fraction of the light cylinder. A size as large as, e.g., 50 neutron star radii (Kijak & Gil 2003) would decrease $T_{\rm b}$ by three orders of magnitude. This would not put into question coherent emission at 400 MHz and in ALMA Band 3 and, possibly, in Band 7. Therefore, most likely, coherence in the millimeter/submillimeter domain is maintained. As a consequence, the transition to incoherent emission processes must occur at frequencies above 343 GHz, i.e., at wavelengths shorter than 0.87 mm, somewhere between the submillimeter and the near-IR. As for the coherent processes responsible for the emission between 400 MHz and 343 GHz, none can be convincingly favored against another (e.g., Eilek & Hankins 2016; Melrose 2017).

We also compared the ALMA PL spectrum of the Vela pulsar with the extrapolation of the flat UV–optical–near-IR PL spectrum (Zyuzin et al. 2013) $F_\nu \propto \nu^{0.01 \pm 0.0}$ (Figure 2). The latter spectrum also encompasses the flux density ($1.35 \pm 0.06\,\mu$Jy) measured in the K_S band (138.8 THz) for the pulsar (Zyuzin et al. 2013). This flat spectral component is likely due to incoherent magnetospheric synchrotron radiation (SR) by electron–positron pairs. If this is the case, then we can estimate how far the SR component can reach toward lower frequencies. When extrapolated to Band 7, its flux density level would fall short by a factor of $\sim$50 below the ALMA point, suggesting the brightness temperature around 10^{13} K, i.e., still exceeding the temperature limit of $\sim 10^{12}$ K due to the inverse Compton catastrophe (Kellermann & Pauliny-Toth

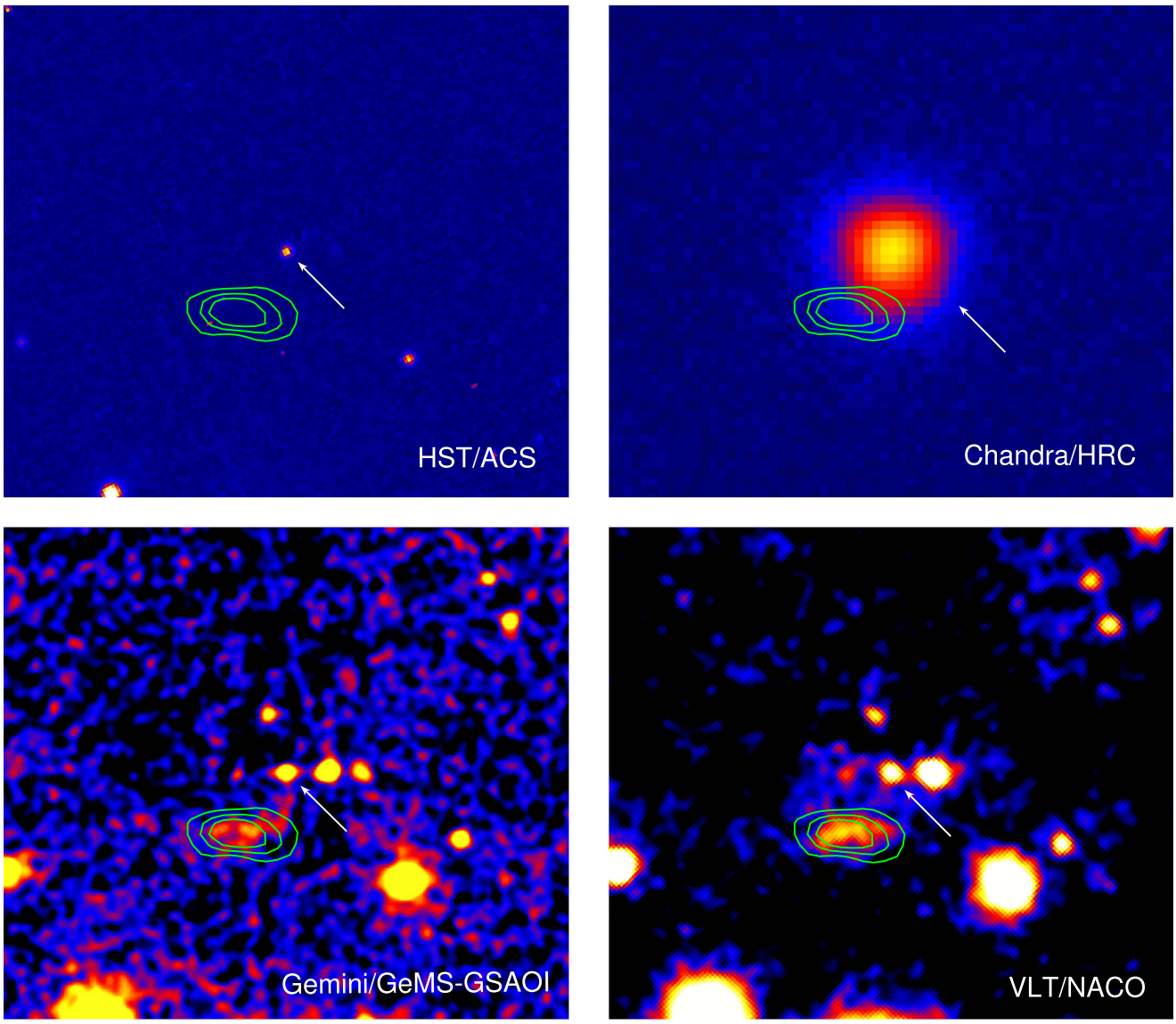

Figure 3. ALMA Band 7 intensity contours (in green) of the nebula close to the Vela pulsar (see Figure 1) superimposed on the *HST*/ACS, *Chandra*/HRC, Gemini/GeMS-GSAOI, and VLT/NACO images of the field, top left to bottom right. In all panels, the angular dimension is $10'' \times 10''$ and the arrow indicates the pulsar. The time baseline between the Gemini, VLT, and ALMA observations ($\sim$3 years), together with the spatial resolution ($0\overset{''}{.}8$) and astrometry accuracy ($0\overset{''}{.}123$) of the Band 7 image, are not sufficient to appreciate a relative angular displacement of the nebula comparable to that predicted for the pulsar ($\approx 0\overset{''}{.}2$) as a results of its proper motion.

1969). We conclude, therefore, that the UV–optical–near-IR spectrum due to incoherent SR does not extend to the submillimeter range but it should turn over somewhere between the mid- and far-IR due to either synchrotron self-absorption or low-energy cutoff. Finally, we compared the ALMA PL spectrum of the Vela pulsar with the extrapolation of the mid-IR flux densities (Danilenko et al. 2011) to the millimeter/submillimeter region.[10] The ALMA spectrum is clearly below such an extrapolation (Figure 2), which indicates a turnover in the wavelength interval between $\sim$0.87 mm and 5.8 μm (343 and 51688 GHz, respectively).

Changes in the PL slope from the UV to the radio are also seen in the Crab pulsar (e.g., Danilenko et al. 2011). Whether these changes reflect emission from a different population of relativistic particles, a difference in the location of the emission regions in the magnetosphere, or different emission mechanisms can only be clarified by further studies.

We also note that the slope of the ALMA spectrum rules out a possibility that the mid-IR-to-submillimeter spectrum of the Vela pulsar is described by a low-temperature blackbody, with the ALMA fluxes along its Rayleigh–Jeans tail, which could be associated with emission from a cold debris disk left over from the supernova explosion (Özsükan et al. 2014). The nondetection of a disk around the Vela pulsar may support the hypothesis that high inclination angles α between the pulsar magnetic dipole and spin axis yield unfavorable conditions for such disks to be stable. A compilation of the values of α, based on the combination of both radio and γ-ray observations, is given in Barnard et al. (2016) and shows that they are mostly close to 70°. A value

[10] The *Spitzer* mid-IR flux measurements at 3.6 and 5.8 μm (83275 and 51688 GHz, respectively) are uncertain owing to the possible contamination of a structure at $1\overset{''}{.}4$, which cannot be spatially resolved from the pulsar at the *Spitzer* angular resolution (Zyuzin et al. 2013).

of $\alpha \sim 53°$ is inferred by Johnston et al. (2005) but using radio observations only.

4.2. The Nebula

We compared the ALMA Band 7 image with those taken with the Advanced Camera for Surveys (ACS) on board *HST* and the 606W filter ($\lambda = 0.59\ \mu$m; $\Delta\lambda = 0.25\ \mu$m), see Figure 3 (top left). There is no stellar object close to the position of the nebula. Therefore, it is unlikely that it is associated with the unresolved contribution of background stars. We note that the position of the nebula emission centroid with respect to the pulsar position lies close to the axis of symmetry of the X-ray PWN observed by *Chandra*, which is at a position angle of $310° \pm 1.°5$, computed east from north (Helfand et al. 2001). To investigate a possible association with the PWN, we compared the ALMA Band 7 image with a *Chandra* image (Figure 3, top right) taken with the High Resolution Camera in imaging mode (HRC-I; Obs. ID 1966). However, even exploiting the sharp *Chandra* PSF, the nebula is too close to the pulsar to resolve possible X-ray features on an angular scale as small as $1.''4$.

Interestingly, based on Gemini-south K_s-band images taken in 2013 January with the Gemini Multi-conjugate Adaptive Optics System (GeMS) and the Gemini South Adaptive Optics Imager (GSAOI) Zyuzin et al. (2013) claimed the detection of an extended structure, also at $\sim 1.''4$ southeast from Vela and aligned closely with its PWN symmetry axis, which they interpreted as a counter-jet protruding from the pulsar. To confirm the Gemini detection, we used archival,[3] unpublished, K_s-band high spatial resolution images of the Vela pulsar field taken between 2012 December and 2013 February with the S54 camera ($54'' \times 54''$; $0.''054$ pixel scale) of the Nasmyth Adaptive Optics System (NAOS) Near-IR Imager and Spectrograph (CONICA)—NACO—at the VLT. Figure 3 (bottom left) shows the Gemini/GeMS-GSAOI K_s-band image compared with the almost contemporary VLT/NACO K_s-band one (bottom right). The same structure seen in the former image is also detected at exactly the same position in the latter, confirming that it is real and not due to a background fluctuation.

The nebula seen in the ALMA Band 7 image is similar in morphology to the structure detected in the K_s-band images and is spatially coincident with it (Figure 3, bottom), meaning that they are the same object. One possibility is that it would form from a jet-like activity from the pulsar, perhaps a counter-jet (Zyuzin et al. 2013) like that observed in the X-ray PWN. At the distance of the Vela pulsar of 287^{+19}_{-17} pc (Dodson et al. 2003), the Band 7 luminosity of the nebula would be $\sim 6 \times 10^{25}$ erg s^{-1}, which is a tiny fraction of the pulsar rotational energy loss rate $\dot{E} = 6.96 \times 10^{36}$ erg s^{-1}. An emission knot like that observed close to the Crab pulsar (Hester et al. 1995) might be another possibility. Very little can be said on the nebula spectrum, with only a direct K_s-band detection (2.34 ± 0.17; μJy; Zyuzin et al. 2013) to be compared with our Band 7 one ($278 \pm 33\ \mu$Jy), which corresponds to a PL with $\alpha = -0.79 \pm 0.02$.

5. Summary and Conclusions

We detected the Vela pulsar with ALMA at frequencies of 97.5, 145, 233, and 343.5 GHz. This is the first detection of a pulsar ever obtained with ALMA. We found that the pulsar spectrum is fitted by a PL with spectral index $\alpha = -0.93 \pm 0.16$. Our observations show that the brightness temperature is still quite high with values of $\approx 10^{27}$ K at 300 MHz down to 10^{15} K at 343 GHz (0.87 mm), for an emission region of the same size as the pulsar, indicating that coherence is maintained.

Finding pulsations at the radio period, or placing strong constraints on their presence, in one or more of the ALMA bands by exploiting the phased-array mode would be a strong test for a connection or lack thereof between the millimeter/submillimeter emission and the radio emission from the comparison of the pulse profiles. If the ALMA flux is pulsed, with a pulse profile similar to the radio one, this would imply that the radio emission still extends to the millimeter/submillimeter region. At the same time, detecting pulsations would be a firm identification evidence.

Our results show that the transition to incoherent emission processes, which are expected to dominate at least from the near-IR up to the highest energies, must occur at wavelengths shorter than 0.87 mm, somewhere between the submillimeter and the near-IR. Measuring the mid-IR spectrum of the Vela pulsar between $\sim$0.005 mm and $\sim$0.03 mm with the *James Webb Space Telescope* (*JWST*) would then be crucial to constrain the wavelength range where such a transition occurs.

Our ALMA observations, together with archival VLT ones in the near-IR, also confirmed the existence of an extended emission structure (the "nebula") at $1.''4$ from the pulsar (Zyuzin et al. 2013). *JWST* observations would better characterize its spectrum in the near-IR/submillimeter. Monitoring in time the position, brightness, and morphology of the nebula would also provide information on its origin and its connection with the pulsar.

We dedicate this work to our dear friend Giovanni F. Bignami, who passed away unexpectedly when this manuscript was in preparation. Nanni, as he was known to his friends, has played a major role in promoting multi-wavelength observations of pulsars and authored many inspirational works on the study of the Vela pulsar. This Letter makes use of the following ALMA data: ADS/JAO.ALMA#2015.1.01104.S. ALMA is a partnership of ESO (representing its member states), NSF (USA) and NINS (Japan), together with NRC (Canada), *MOST* and ASIAA (Taiwan), and KASI (Republic of Korea), in cooperation with the Republic of Chile. The Joint ALMA Observatory is operated by ESO, AUI/NRAO, and NAOJ. Based on observations made with ESO Telescopes at the La Silla Paranal Observatory under program ID 090.D-0425(A). R.P.M. acknowledges financial support from an "Occhialini Fellowship." B.R. acknowledges financial support by the National Science Centre Grant DEC-2011/02/A/ST9/00256. We thank Simon Johnston for providing information on the radio flux densities of Vela and Patrizia Caraveo for her careful reading of the manuscript.

Facilities: ALMA, VLT.

ORCID iDs

R. P. Mignani https://orcid.org/0000-0002-8685-583X
B. Rudak https://orcid.org/0000-0003-0452-3805
M. Burgay https://orcid.org/0000-0002-8265-4344

References

Acero, F., Ackermann, M., Ajello, M., et al. 2015, ApJS, 218, 23
Barnard, M., Venter, C., & Harding, A. K. 2016, ApJ, 832, 107

[11] http://www.eso.org/archive

Danilenko, A. A., Zyuzin, D. A., Shibanov, Yu. A., & Zharikov, S. V. 2011, MNRAS, 415, 867
Dodson, R., Legge, D., Reynolds, J. E., & Mc Culloch, P. M. 2003, ApJ, 596, 1137
Eilek, J. A., & Hankins, T. H. 2016, JPlPh, 82, 635820302
Fomalont, E., van Kempen, T., Kneissl, R., et al. 2014, Msngr, 155, 19
Harnden, F. R., & Gorenstein, P. 1973, Natur, 241, 107
Helfand, D. J., Gotthelf, E. V., & Halpern, J. P. 2001, ApJ, 556, 380
Hester, J. J., Scowen, P. A., Sankrit, R., et al. 1995, ApJ, 448, 240
Jankowski, F., van Straten, W., Keane, E. F., et al. 2018, MNRAS, 473, 4436
Johnston, S., Hobbs, G., Vigeland, S., et al. 2005, MNRAS, 364, 1307
Johnston, S., Karastergiou, A., & Willet, K. 2006, MNRAS, 369, 1916
Keith, M. J., Johnston, S., Levin, L., & Bailes, M. 2011, MNRAS, 416, 346
Kellermann, K. I., & Pauliny-Toth, I. I. K. 1969, ApJL, 155, L71
Kijak, J., & Gil, J. 2003, A&A, 397, 969
Large, M. I., Vaughan, A. E., & Mills, B. Y. 1968, Natur, 220, 340
Lasker, B. M. 1976, ApJ, 203, 193
Leung, G. C. K., Takata, J., Ng, C. W., et al. 2014, ApJL, 797, L13
Manchester, R. N., Hobbs, G. B., Teoh, A., & Hobbs, M. 2005, AJ, 129, 1993
Manzali, A., De Luca, A., & Caraveo, P. A. 2007, ApJ, 669, 570
Melrose, D. 2017, RvMPP, in press (arXiv:1707.02009)
Michel, C. F. 1991, Theory of Neutron Star Magnetospheres (Chicago, IL: Univ. Chicago Press)
Özsükan, G., Ekşi, K. Y., Hambaryan, V., et al. 2014, ApJ, 796, 46
Pacini, F. 1968, Natur, 219, 145
Romani, R. W., Kargaltsev, O., & Pavlov, G. G. 2005, ApJ, 627, 383
Shibanov, Yu. A., Koptsevich, A. B., Sollerman, J., & Lundqvist, P. 2003, A&A, 406, 645
Temim, T., Gehrz, R. D., Woodward, C. E., et al. 2009, AJ, 137, 5155
Thompson, D. J., Fichtel, C. E., Kniffen, D. A., & Ögelman, H. B. 1975, ApJL, 200, L79
Wallace, P. T., Peterson, B. A., Murdin, P. G., et al. 1977, Natur, 266, 692
Zyuzin, D., Shibanov, Yu., Danilenko, A., Mennickent, R. E., & Zharikov, S. 2013, ApJ, 775, 101